scientific reports

Check for updates

OPEN

On hybrid nanofluid Yamada-Ota and Xue flow models in a rotating channel with modified Fourier law

Muhammad Ramzan[1]✉, Hina Gul[1], M. Y. Malik[2], Dumitru Baleanu[3,4,5] & Kottakkaran Sooppy Nisar[6]

The present study analyzes the comparison of the Xue and Yamada-Ota models for a hybrid nanoliquid flow in porous media occurring amidst a rotating channel with surface catalyzed reaction. Here, the hybrid nanofluid flow is studied under the effect of Cattaneo Christov (C–C) heat flux and homogenous heterogeneous (Homo-Hetero) chemical reaction with entropy generation minimization analysis. The assumptions of the viscosity of hybrid nanomaterial fluid and variable thermal conductivity are added characteristics to the inimitability of the flow model. Two kinds of nanoparticles, namely single-wall carbon nanotubes and multi-wall carbon nanotubes with ethylene glycol (EG) as the base fluid are considered. Carbon nanotubes possess diverse applications in daily life including energy storage, drug delivery, cancer treatment, tissue generation, platelet activation, magnetic force microscopy, and microwave absorption, etc. Similarity transformations are utilized to translate the modeled problem into the coupled ordinary differential equations. This system of ordinary differential equations is addressed numerically. The graphical outcomes are scrutinized by utilizing the MATLAB software bvp4c function. The results revealed that the velocity profile decreases for the higher rotation parameter while increases for the escalated slip parameter. Furthermore, the fluid concentration and temperature are on the decline for higher surface catalyzed reaction and thermal relaxation parameters respectively.

List of symbols

a_0, e, a, b	Dimensional constant
M	Thermal slip parameter
s_1	Slip coefficient
L	Length of the nanoparticles
k_{HNF}	Thermal conductivity of nanofluid
T_h	Temperature on wall
Br	Brinkman number
S	Velocity slip parameters
Q	Heat gen/abs parameter
μ_{HNF}	Viscosity of hybrid nanofluid
T	Liquid temperature
U_w	Stretching velocity
ϕ_1, ϕ_2	Nanoparticles volumetric
$A*$	Diffusion coefficient of chemical specie
Sc	Schmidt number
k_{bF}	Thermal conductivity (base fluid)
HNF	Hybrid nanoliquid
$\varepsilon_2, \varepsilon_1$	Diffusion parameter and Thermal conductivity
γ	Thermal relaxation parameter

[1]Department of Computer Science, Bahria University, Islamabad 44000, Pakistan. [2]Department of Mathematics, College of Sciences, King Khalid University, Abha 61413, Saudi Arabia. [3]Department of Mathematics, Cankaya University, Ankara 06790, Turkey. [4]Institute of Space Sciences, 077125 Magurele, Bucharest, Romania. [5]Department of Medical Research, China Medical University Hospital, China Medical University, Taichung 40447, Taiwan. [6]Department of Mathematics, College of Arts and Sciences, Prince Sattam Bin Abdulaziz University, Wadi Aldawaser 11991, Saudi Arabia. ✉email: mramzan@bahria.edu.pk

λ	Porosity parameter
Ω	Angular velocity
Ω_2	Temperature ratio parameter
ν	Kinematic viscosity
K_{vs}	Surface catalyze reaction
k	Chemical reaction parameter
ρ_{s_1}, ρ_{s_2}	Density of nanoparticles
λ	Permeability parameter
Ns	Total entropy generation
k_s	Coefficient of heterogeneous reaction
$k*$	Porosity coefficient
Q_0	Heat generation/absorption coefficient
C_f	Drag force
A_0	Uniform suction
R	The radius of the nanoparticles
$(\rho c_p)_{HNF}$	The ratio of heat capacity
Pr	Prandtl number
ε	Suction/injection parameter
Re	Local Reynolds number
k_1	Chemical reaction parameter
T	Viscous stress tensor
ρ_{HNF}	Density of hybrid nanofluid
Re	Reynold's number
F	Fluid
(u, v, w)	Components of velocities
T_0	Diffusive temperature
ν_f	Kinematic viscosity
D_A,D_B	Diffusion coefficients
κ_∞	Free stream thermal conductivity
K_s	Heterogeneous reaction parameter
k_p	Thermal conductivity of nanoparticles
L_1, L_2	Diffusion parameters
λ_2	Thermal relaxation time
δ	The ratio of the diffusion coefficient
c_p	Specific heat
k_{s_1}, k_{s_2}	Thermal conductivity of nanoparticles
S_0'''	Characteristic entropy generation
τ_w	Shear stress
S_G'''	Entropy generation rate
Be	Bejan number

Carbon nanotubes (CNTs) were first time devised in 1991. CNTs possess a diameter of 0.7–50 nm, are thin cylinders formed of pure carbon. The role of CNTs is essential in numerous modern applications consist of composite materials, nanotechnology, conductive plastics, and atomic force microscope, etc. Two famous types of CNTs, i.e., single walls (SWCNTs) and multi-wall (MWCNTs) are identified in the literature. Significant importance is given by the researchers centering CNTs. Acharya et al.[1] introduced the rotating MHD flow amalgamated with CNTs past a stretching surface. To construct the numerical solution of the non-linear flow problem, the RK-4 procedure is adopted. It is comprehended that for large radiation parameter estimates, the thermal profile increases. Unsteady squeezing CNTs immersed MHD nanofluid flow with viscous dissipation, and entropy generation in a rotating channel is inspected by Dawar et al.[2]. Kumar et al.[3] explored the combined impacts of heat radiation and Hall current on a 3D Micropolar nanoliquid flow with submerged CNTs between two rotating sheets. The physical model characteristics of heat transfer and CNTs immersed nanoliquid flow in an asymmetric permeable channel are studied by Pandit et al.[4]. The wavelet collocation process is used for numerical results. The characteristics of CNTs nanoliquid squeezing flow in three dimensional with the lower stretching wall in a rotating channel is investigated numerically by Khan et al.[5]. The numerical technique known as the Runge–Kutta-Fehlberg (RKF) method to address the resulting equations is engaged here. Lately, the flow of the nanofluid with submersed CNTs in varied geometries may be found in[6–10].

It is a very much understood reality that the transfer of heat phenomenon occurs owing to temperature inconsistency amidst two distinct objects or within an entity. For almost one century, the Fourier law (conduction of heat)[11] was taken as a general principle for heat transfer processes. But later it is realized that in Fourier law if an issue occurs at the beginning that will carry out throughout the entire process and it opposes the causality principle. To answer this matter Cattaneo[12] implanted the thermal relaxation time term in the typical Fourier's law which empowers the transfer of heat by the method of propagation of thermal waves with controlled speed and it was difficult to obtain a single heat equation. Later on, Christov updated the Cattaneo model and got a single equation for the temperature field. This improved model[13] is categorized as the Cattaneo-Christov (C–C) heat flux model. Thermal stratification and C–C heat flux with base fluid EG and immersed CNTs nanofluid flow in rotating frame discussed by Ramzan et al.[14]. The bvp4c MATLAB technique for a numerical solution is used here. It is noticed that the thermal profile reduces for greater stratification parameter. Hayat et al.[15] introduced

C–C heat flux squeezed flow in a rotating frame. The series solutions for temperature and velocity distributions are formed by using the Homotopy Analysis Method. Karim and Samad[16] discussed the influence of Brownian diffusion with C–C heat flux on elastic viscous squeezing nanoliquid flow and double slip impact in a channel. Some latest attempts about nanoliquid can be witnessed through[17–21].

Hybrid nanoliquid, is the developing field of engineering that has trapped the eye of copious researchers who were looking at ways to enhance the productivity of cooling processes in the industry. Nanoliquid is a fluid that is made by the propagation of strong particles with sizes less than 100 nm in fluids. A nanoliquid with low thermal conductivity is one of its striking parameters that can restrict the performance of the heat transfer. Due to this shortcoming, normal heat transport fluids such as H_2O and $(CH_2OH)_2$, and motor oil have limited heat transfer capabilities and are therefore unable to meet today's cooling requirements. Suspended nanoparticles can improve the fluid flow and heat transfer features of the base liquid. Extensive studies are conducted by the researchers to highlight numerous aspects of nanofluid flows. Gul et al.[22] examined nanoliquid flow in a rotating channel with C–C heat flux containing CNTs with $(CH_2OH)_2$ as a base fluid. Ramzan et al.[23] investigated the nanoliquid flow with the effect of C–C heat flux under the influence of the H–H reaction. Hayat et al.[24] introduced nanoliquid with CNTs and Darcy-Forchheimer. They utilized water as a base fluid. Ramzan et al.[25] initiated the C–C impact on Tangent hyperbolic liquid flow amalgamated with second-order slip. They utilized the Runge–Kutta Fehlberg technique to tackle the problem. Some more explorations about nanoliquid may be found in[26–32].

The aforementioned literature review discloses that copious studies are available that focus on the flow of nanofluids with immersed CNTs in numerous geometries. Nevertheless, limited explorations may be quoted with hybrid nanoliquid flows with engrossed CNTs and EG as a customary liquid. But no study until now is conducted that deliberated the comparative analysis of hybrid nanofluid models *i.e.,* Xue and Yamada and Ota amidst a permeable rotating channel with C–C heat flux amalgamated with the Homo-Hetero reactions and surface catalyzed reaction. The surface catalyzed reaction triggers the chemical reaction in a comparatively lesser time. Furthermore, the fluid models discussed in the literature assumed constant viscosity and thermal conductivity but in real engineering applications, both are considered as a variable. Here, the uniqueness of the fluid model is also augmented by considering both impacts as a variable which makes this study more realistic. The numerical results of the problem are obtained by using the bvp4c MATLAB technique. Through this investigation, we intend to answer the following questions:

i. How fluid velocity is influenced by the rotation and the slip impacts?
ii. What are the impacts of the surface-catalyzed parameter and the thermal relaxation parameter on the fluid concentration and the temperature respectively?
iii. Which hybrid nanofluid model is more dominating?
iv. How entropy generation rate is affected by the porosity parameter and the Reynolds number?
v. What are the effects of the Prandtl and Schmidt numbers of the heat transfer and mass transfer rates respectively?

Mathematical formulation

Assume the flow of hybrid nanofluid (SWCNTs-MWCNTs/EG) with Yamada-Ota and Xue models between two parallel plates. The whole system rotates about the *y*-axis with fixed angular velocity ($\Omega_)$. The value of Ω specifies the direction of rotation of both lower and upper plates, that is for $\Omega > 0$ both plates rotate in the same direction and for $\Omega < 0$ both plates are rotated in the opposite direction while for static plates, we assign the value of $\Omega = 0$. And both plates are distance "*h*" apart. The lower plate moves faster as compared to the upper plate with $U_w = ax$ ($a > 0$). The positions of the upper and lower plates are at $y = h$, and $y = 0$, respectively. The coordinate system is taken in such a way that plates are parallel to the *x-axis*, and the *y-axis* is perpendicular to the plates (Fig. 1).

For rotating flow, the momentum governing equation is[33–35]:

$$\rho_{HNF}\left(\frac{dV}{dt} + 2\Omega \times v + \Omega \times (\Omega \times r)\right) = div\tau. \tag{1}$$

The governing boundary layer equations under the impact of C–C heat flux are represented as:

$$u_X + v_Y = 0, \tag{2}$$

$$\rho_{HNF}(uu_X + vu_Y + 2\Omega w) = -P_X + \mu_{HNF}(u_{XX} + u_{YY}) - \frac{\mu_{HNF}}{k^*}u \tag{3}$$

$$\rho_{HNF}(uv_X + vv_Y) = -P_Y + \mu_{HNF}(v_{XX} + v_{YY}), \tag{4}$$

$$\rho_{HNF}(uw_X + vw_Y - 2\Omega u) = \mu_{HNF}(w_{XX} + w_{YY}) - \frac{\mu_{HNF}}{k^*}w. \tag{5}$$

The modified pressure is defined as $P = p - \frac{\Omega^2 X^2}{2}$. Mathematically the heat transfer phenomenon can be expressed as:

$$(\rho c_p)_{HNF}(uT_X + vT_Y) = -\nabla.\mathbf{q} + \frac{Q_0(T - T_0)}{(\rho c_p)_{HNF}}, \tag{6}$$

where **q** is the heat flux which satisfies the following relationship:

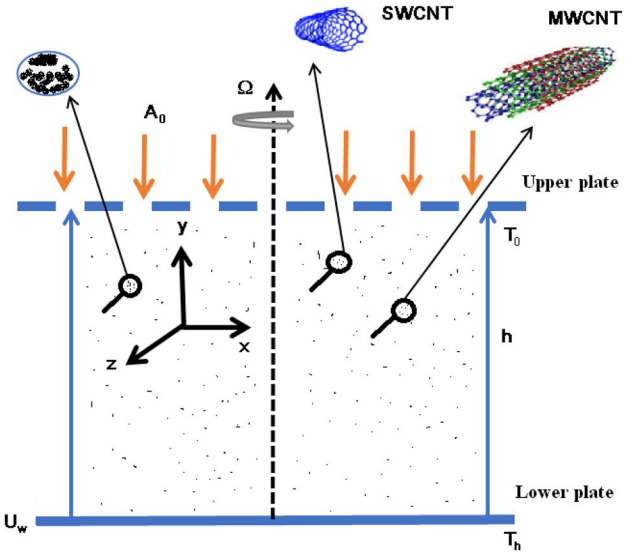

Figure 1. Flow problem[33].

$$\mathbf{q} + \lambda_1(\mathbf{q}_t - \mathbf{q}.\nabla V + V.\nabla\mathbf{q} + (\nabla.V)\mathbf{q}) = -k_{HNF}(T)\nabla T. \tag{7}$$

Removing $\mathbf{q}$ from (6) and (7) following Hayat[15], we get:

$$\begin{aligned} uT_X + vT_Y = \frac{\partial}{\partial y}\left(\frac{k_{HNF}(T)}{(\rho c)_{HNF}}T_Y\right) - \lambda_2(u^2T_{XX} + v^2T_{YY} + 2uvT_{XY} + (uu_X + vu_Y)T_X \\ + ((uv_X + vv_Y)T_Y) + \frac{Q_0(T - T_0)}{(\rho c_p)_{HNF}}, \end{aligned} \tag{8}$$

$$ua_X + va_Y = \frac{\partial}{\partial y}(D_A(a)a_Y) - k_1ab^2 - Sk_sa, \tag{9}$$

$$ub_X + vb_Y = \frac{\partial}{\partial y}(D_B(b)b_Y) + k_1ab^2 + Sk_sa. \tag{10}$$

The associated B. C's are presented as:

$$u = U_w + s_1\frac{\mu_{HNF}}{\rho_{HNF}}u_Y, v = 0, w = 0, T = T_h + \chi_1\frac{k_{HNF}(\widehat{T})}{k_F}T_Y, D_Aa_Y = k_sa, D_Bb_Y = -k_sa \text{ at } y = 0, \tag{11}$$

$$u = 0, v = -A_0, w = 0, T = T_\infty, \ a \to a_0, b \to 0, \text{ as } y \to h, \tag{12}$$

where $-A_0$ is represented the uniform suction/injection for injection ($-A_0 < 0$), and the suction ($-A_0 > 0$), velocity at the upper wall. The temperature-dependent thermal conductivity is specified as:

$$K(T) = \kappa_\infty\left(1 + \varepsilon_1\frac{T - T_0}{T_h - T_0}\right), \tag{13}$$

with κ_∞ is the free stream thermal conductivity. Here, $\varepsilon_1 > 0$ expressing for gas while liquid characteristics are represented by $\varepsilon_1 < 0$, with ε_1 is of unit dimension.

Also, $D_A(a)$ is the diffusion coefficient (concentration-dependent) of chemical species A^*, and $D_B(b)$ is the diffusion coefficient (concentration-dependent) of chemical specie B^* and are defined as follows:

$$D_A(a) = D_A\left[1 + \varepsilon_2\left(\frac{a}{a_0}\right)\right], \tag{14}$$

$$D_B(b) = D_B\left[1 + \varepsilon_2\left(\frac{b}{a_0}\right)\right], \tag{15}$$

where ε_2 is of unit dimension.

Tables 1, 2, and 3 describe the thermophysical features of the hybrid nanofluid flow models, and CNTs/base fluid respectively.

Density	$\rho_{HNF} = \rho_F(1-\phi_2)\left((1-\phi_1)+\phi_1\left(\frac{\rho_{s1}}{\rho_F}\right)\right)+\phi_2\rho_{s_2}, \frac{\rho_{HNF}}{\rho_F} = A.$
Heat Capacity	$(\rho c_p)_{HNF} = \phi_2(\rho c_p)_{s_2} + (1-\phi_2)(\rho c_p)_F\left\{\phi_1\frac{(\rho c_p)_{s_1}}{(\rho c_p)_F} + [(1-\phi_1)]\right\}$ $\frac{(\rho c_p)_{HNF}}{(\rho c_p)_F} = C$
Variable viscosity	$\mu_{HNF} = \frac{\mu_F}{(1-\phi_1)^{2.5}(1-\phi_2)^{2.5}}, \quad \frac{\mu_{HNF}}{\mu_F} = B.$
Thermal conductivity	$\frac{k_{HNF}(T)}{k_{bF}} = \frac{(n-1)k_{bF}+k_{s_2}-(k_{bF}-k_{s_2})(n-1)\phi_2}{(n-1)k_{bF}+k_{s_2}+(k_{bF}-k_{s_2})\phi_2}(1+\varepsilon_1\theta)$ $\frac{k_{bF}}{k_F} = \frac{(n-1)k_F+k_{s_1}-(n-1)\phi_1(k_F-k_{s_1})}{k_F(n-1)+k_{s_1}+\phi_1(k_F-k_{s_1})}, \quad \frac{k_{HNF}}{k_{bF}} = E, \frac{k_{bF}}{k_F} = D$
Xue-model	$\frac{k_{HNF}}{k_{bF}} = \frac{1-\phi_2+2\phi_2\left(\frac{k_{s_2}}{k_{s_2}-k_{bF}}\right)\ln\frac{k_{s_2}+k_{bF}}{2k_{bF}}}{1-\phi_2+2\phi_2\left(\frac{k_{s_2}}{k_{s_2}-k_{bF}}\right)\ln\frac{k_{s_2}+k_{bF}}{2k_{bF}}},$ $\frac{k_{bF}}{k_F} = \frac{1-\phi_1+2\phi_1\left(\frac{k_{s_1}}{k_{s_1}-k_F}\right)\ln\frac{k_{s1}+k_F}{2k_F}}{1-\phi_1+2\phi_1\left(\frac{k_F}{k_{s1}-F}\right)\ln\frac{k_{s1}+k_F}{2k_F}}.$
Yamada-Ota model	$\frac{k_{HNF}}{k_{bF}} = \frac{1+\frac{k_{bF}}{k_{s_2}}\frac{L}{R}\phi_2^{0.2}+\left(1-\frac{k_{bF}}{k_{s_2}}\right)\phi_2\frac{L}{R}\phi_2^{0.2}+2\phi_2\left(\frac{k_{s_2}}{k_{s_2}-k_{bF}}\right)\ln\frac{k_{s_2}+k_{bF}}{2k_{s_2}}}{1-\phi_2+2\phi_2\left(\frac{k_{bF}}{k_{s_2}-k_{bF}}\right)\ln\frac{k_{s_2}+k_{bF}}{2k_{bF}}},$ $\frac{k_{bF}}{k_F} = \frac{1+\frac{k_F}{k_{s_1}}\frac{L}{R}\phi_1^{0.2}+\left(1-\frac{k_F}{k_{s_1}}\right)\phi_1\frac{L}{R}\phi_1^{0.2}+2\phi_1\left(\frac{k_{s_1}}{k_{s_1}-k_F}\right)\ln\frac{k_{s_1}+k_F}{2k_{s_1}}}{1-\phi_1+2\phi_1\left(\frac{k_F}{k_{s_1}-k_F}\right)\ln\frac{k_{s_1}+k_F}{2k_F}}.$

Table 1. Thermophysical attributes of hybrid nanoliquid[34].

Physical properties	Ethylene glycol	SWCNT	MWCNT
$\rho\left(\frac{kg}{m^3}\right)$	1115	2600	1600
$c_p\left(\frac{J}{kg.K}\right)$	2430	425	796
$K\left(\frac{W}{m.K}\right)$	0.253	6600	3000

Table 2. Thermophysical traits of Ethylene glycol and CNTs[14].

		$C_f\sqrt{Re_x}$	
Re	λ	Yamada-Ota model	Xue model
1.5	0.5	3.2545	3.2526
2.5		3.2981	3.2965
3.5		3.3421	3.3405
	0.1	3.2036	3.2019
	0.4	3.2416	3.2401
	0.7	3.2803	3.2789

Table 3. Numerical results of $C_f\sqrt{\mathrm{Re}_x}$ for Re and λ.

The Similarity transformations are characterized as:

$$u = exf'(\eta),\ v = -ehf(\eta),\ v = -ehf(\eta),\ \theta(\eta) = \frac{T-T_0}{T_h-T_0},\ \phi = \frac{a}{a_0}, H = \frac{b}{a_0},\ \eta = \frac{y}{h}. \tag{16}$$

By invoking the above transformation into the Eqs. (3) - (12), we obtain the following dimensionless equations to obtain the flow profiles.

$$f^{iv} + BA\mathrm{Re}(f'f'' - ff''') - A\Omega g' - \lambda f' = 0, \tag{17}$$

$$g'' - AB\mathrm{Re}(gf' - fg') + 2BA\Omega f' + \lambda g = 0, \tag{18}$$

$$\frac{ED}{C}\left((1+\varepsilon_1\theta)\theta'' + \varepsilon_1\theta'^2\right) + \Pr \mathrm{Re}\left(\frac{Q}{C}\theta + f\theta' - \gamma(f^2\theta'' + ff'\theta'\right) = 0, \tag{19}$$

$$(1+\varepsilon_2\phi)\phi'' + \phi'^2\varepsilon_2 + \mathrm{Re}Sc(f\phi' - k\phi H^2 - K_{vs}\phi) = 0, \tag{20}$$

$$(1+\varepsilon_2\phi)H'' + H'^2\varepsilon_2 + \mathrm{Re}\frac{Sc}{\delta}(f\,H' + k\phi H^2 + K_{vs}\phi) = 0, \tag{21}$$

$$\begin{gathered} f'(0) = 1 + S\frac{B}{A}f''(0),\ f(0){=}0, g(0) = 0,\ \theta(0) = 1 + M\theta'(0)\frac{k_{HNF}}{k_F}(1+\varepsilon_1\theta), \\ (1+\varepsilon_2\phi)\phi'(0) = K_s\phi(0),\ \ [1+\varepsilon_2 H(0)]H'(0) = -K_s\phi(0), \\ f'(h) = 0, f(h) = \varepsilon,\ g\ (h) = 0,\ \theta\ (h) = 0, \phi(h) = 1, H(h) = 0. \end{gathered} \tag{22}$$

The quantities in the above equations are defined as:

$$\begin{gathered} \gamma = \lambda_2 e, k = \frac{k_1 a_0^2}{e},\ \mathrm{Re} = \frac{eh^2}{\nu_F}, Q = \frac{Q_0}{c\left(\rho c_p\right)_F}, \varepsilon = \frac{A_0}{eh}, \Pr = \frac{\mu_F c_p}{k_F},\ \Omega = \frac{\gamma h^2}{\nu_F},\ M = \frac{\chi_1}{h},\ S = \frac{s_1\nu_F}{h}, \\ K_{vs} = S_v K_s, K_s = \frac{k_s\sqrt{\nu_F}}{D_A\sqrt{e}} S_v = \frac{SD_A}{e},\ \ \delta = \frac{D_B}{D_A},\ Sc = \frac{\nu_F}{D_A},\ \ K_s = \frac{k_s a_0}{D_B}, \end{gathered} \tag{23}$$

We assume the diffusion coefficients of both chemical species are identical since their sizes are comparable. The following relationship will result from this assumption:

$$H(\eta) + \phi(\eta) = 1, \tag{24}$$

$$2(1+\varepsilon_2\phi)\phi'' + 2\varepsilon_2\phi'^2 + \mathrm{Re}Sc(2f\phi' - K\phi(1-\phi)^2 - K_{vs}\phi = 0, \tag{25}$$

$$(1+\varepsilon_2\phi)\phi'(0) = K_s\phi(0),\ \ \phi(h) = 1. \tag{26}$$

Drag force coefficient, mass transfer rate, and Nusselt number are defined by:

$$C_f = \frac{2\tau_w}{\rho_{HNF}U_w^2},\ Sh_x = \frac{hj_w}{D_B(C_w - C_\infty)},\ Nu_r = \frac{hq_w}{k_\infty(T_w - T_\infty)}, \tag{27}$$

with

$$\tau_w = \mu_{HNF}\left(\frac{\partial u}{\partial y}\right)_{y=0}, q_w = -K(T)\,T_y\big|_{y=0}, j_w = -D_B b_{y=0}. \tag{28}$$

Dimensionless surface drag coefficient, mass transfer rate, and heat transfer rate are:

$$C_f\sqrt{\mathrm{Re}_x} = \left(\frac{1}{(1-\varphi_1)^{2.5}(1-\varphi_2)^{2.5}}\right)f''(\eta)\Big|_{\eta=0}, Sh_x = -\phi'(0), Nu_x = -(1+\varepsilon\theta)\theta'(0). \tag{29}$$

Entropy generation analysis

The volumetric entropy generation is represented as[36]:

$$\begin{aligned} S'''_{GEN} = {} & \frac{k_{HNF}}{T_0^2}T_Y^2 + \frac{\mu_{HNF}}{T_0}u_Y^2 + \frac{\mu_{HNF}}{T_0 k*\Omega_1}u^2 + \frac{RD_A(a)}{T_0}a_Y T_Y \\ & + \frac{RD_A(a)}{a_0}(a_Y)^2 + \frac{RD_B(b)}{T_0}b_Y T_Y + \frac{RD_B(b)}{a_0}(b_Y)^2. \end{aligned} \tag{30}$$

The entropy generation in the non-dimensional form is appended below:

$$N_S = \frac{S'''_{GEN}}{S'''_0} = \left(\begin{array}{l} \Omega_2 ED(1+\varepsilon\theta)\left(\theta'(\eta)\right)^2 + BBr(f''^2(\eta) + \lambda * f'^2(\eta)) \\ \quad + L_1(1+\varepsilon_2\phi)\phi'\theta' + \dfrac{L_1}{\Omega_2}\phi'^2 + L_2(1+\varepsilon_2(1-\phi)\phi'\theta' + \dfrac{L_2}{\Omega_2}\phi'^2 \end{array}\right), \tag{31}$$

where

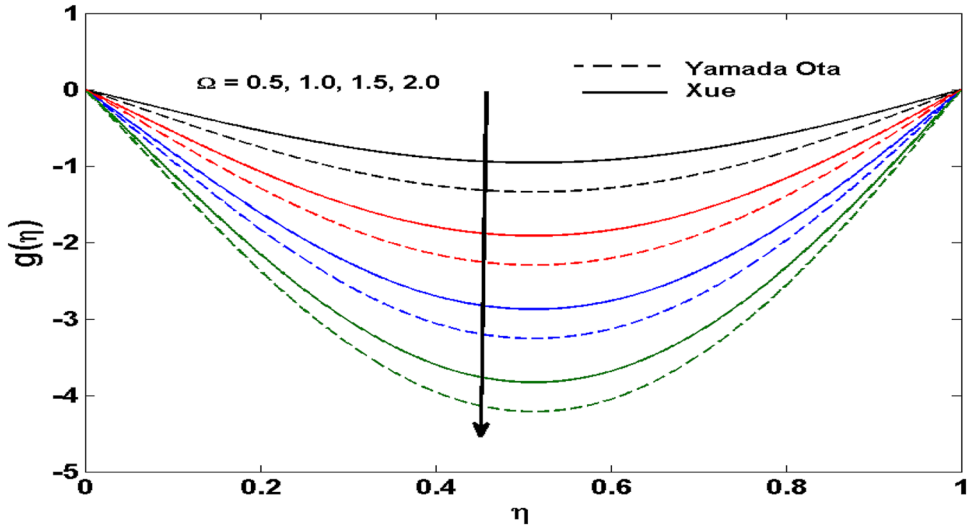

Figure 2. Behaviour of $g(\eta)$ vs Ω. Image generated by using MATLAB 2015a https://www.mathworks.com/help/simulink/release-notes-R2015a.html.

$$S_0''' = \frac{k_F \nabla T}{h^2 T_0},\ Br = \frac{\mu_F U_w^2 h^2}{k_F(T_h - T_0)},\ \Omega_2 = \frac{T_h - T_0}{T_0},\ \lambda* = \frac{\nu_F}{k^* \Omega_1},\ L_1 = \frac{RD_A a_0}{k_F},\ L_2 = \frac{RD_B a_0}{k_F}. \tag{32}$$

The Bejan number (Be) is presented as:

$$Be = \frac{\left(\frac{k_{HNF}}{T_0^2} T_Y^2 + \frac{RD_A(a)}{T_0} a_Y T_Y + \frac{RD_A(a)}{a_0}(a_Y)^2 + \frac{RD_B(b)}{T_0} b_Y T_Y + \frac{RD_B(b)}{a_0}(b_Y)^2\right)}{\left(\frac{k_{HNF}}{T_0^2} T_Y^2 + \frac{\mu_{HNF}}{T_0} u_Y^2 + \frac{\mu_{HNF}}{T_0 k* \Omega_1} u^2 + \frac{RD_A(a)}{T_0} a_Y T_Y + \frac{RD_A(a)}{a_0}(a_Y)^2 + \frac{RD_B(b)}{T_0} b_Y T_Y + \frac{RD_B(b)}{a_0}(b_Y)^2\right)}. \tag{33}$$

In the dimensionless form, the Be is given as:

$$Be = \frac{\left(\Omega_2 ED\left(\theta'(\eta)\right)^2 + L_1(1 + \varepsilon_2\phi)\phi'\theta' + \frac{L_1}{\Omega_2}\phi'^2 + L_2(1 + \varepsilon_2(1-\phi))\phi'\theta' + \frac{L_2}{\Omega_2}\phi'^2\right)}{\left(\begin{array}{l}\Omega_2 ED\left(\theta'(\eta)\right)^2 + CBr(f^{''2}(\eta) + \lambda * f^{'2}(\eta)) + L_1(1 + \varepsilon_2\phi)\phi'\theta' + \frac{L_1}{\Omega_2}\phi'^2 \\ + L_2(1 + \varepsilon_2(1-\phi))\phi'\theta' + \frac{L_2}{\Omega_2}\phi'^2\end{array}\right)}. \tag{34}$$

For a similar solution, the Brinkman number is given by:

$$Br = \frac{\mu_F U_w^2 h^2}{k_F(T_h - T_0)} = \frac{\mu_F x^2 e^2 h^2}{k_F(T_h - T_0)}. \tag{35}$$

To get rid of x in Br, the temperature $T_h(x)$ may be in the form $T_h = T_0 + T_1 x^2$, where T_1 is a constant, Else, the solution found is only locally similar. By utilizing the above-described transformation, Eq. (35) takes the form $Br = \frac{\mu_F e^2 h^2}{k_F T_1}$.

Results with discussion

The Xue and Yamada–Ota are two hybrid nanoliquid models on the velocity, thermal, and concentration profiles are debated here versus the arising parameters slip parameter ($0.1 \le S_1 \le 0.4$), rotation parameter ($0.5 \le \Omega \le 2.0$), Reynolds number ($0.5 \le \mathrm{Re} \le 3.5$), multi-wall nanoparticles volume fraction ($0.005 \le \phi_2 \le 0.02$), thermal slip parameter ($0.5 \le M \le 2.0$), thermal relaxation parameter ($0.5 \le M \le 2.0$), Prandtl number ($1.0 \le \mathrm{Pr} \le 4.0$), thermal conductivity parameter ($0.3 \le \varepsilon_1 \le 0.7$), surface-catalyzed parameter ($0.3 \le K_{VS} \le 0.5$), heterogeneous parameter ($0.3 \le k_s \le 0.6$), heat generation absorption coefficient ($-1.0 \le Q \le 1.0$), porosity parameter ($0.5 \le \lambda* \le 2.0$), and Brinkman number ($0.5 \le Br \le 4.0$). In Fig. 2, the influence of rotation parameter (Ω) on velocity profile $g(\eta)$ is presented. It is observed that for greater estimations of Ω, $g(\eta)$ reduces. It is interesting to notice that the problem is reduced to 2-dimensional flow in a channel when the rotation parameter is not considered. The association of the Reynolds number (Re) with the velocity profiles $g(\eta)$ and $f'(\eta)$ is portrayed in Figs. 3 and 4 respectively. A declining trend is seen for augmented Reynolds number (Re) estimates. Reynolds number (Re) is a dimensionless number that is used in various fluid flow situations to measure the flow pattern. The fluid flow appears to laminar at low Re, while at high Re, the flow of liquids tends to be turbulent. This trend of the fluid velocities versus the higher Reynolds number is according to the physics of the problem. Figure 5 is plotted for thermal profile against the growing values of nanoparticles

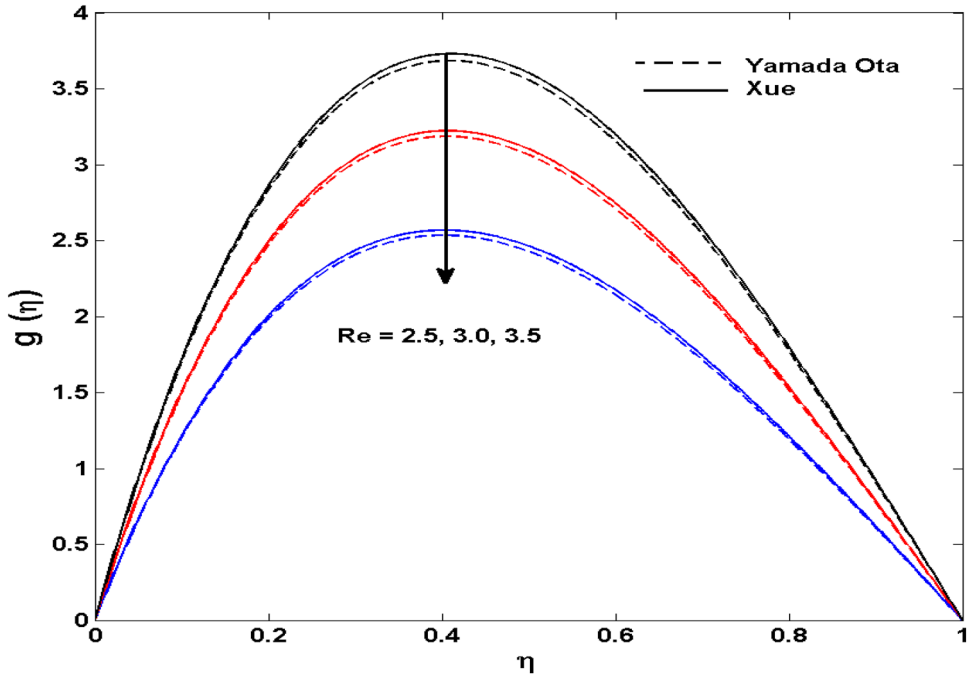

Figure 3. Behaviour of $g(\eta)$ vs Re. Image generated by using MATLAB 2015a https://www.mathworks.com/help/simulink/release-notes-R2015a.html.

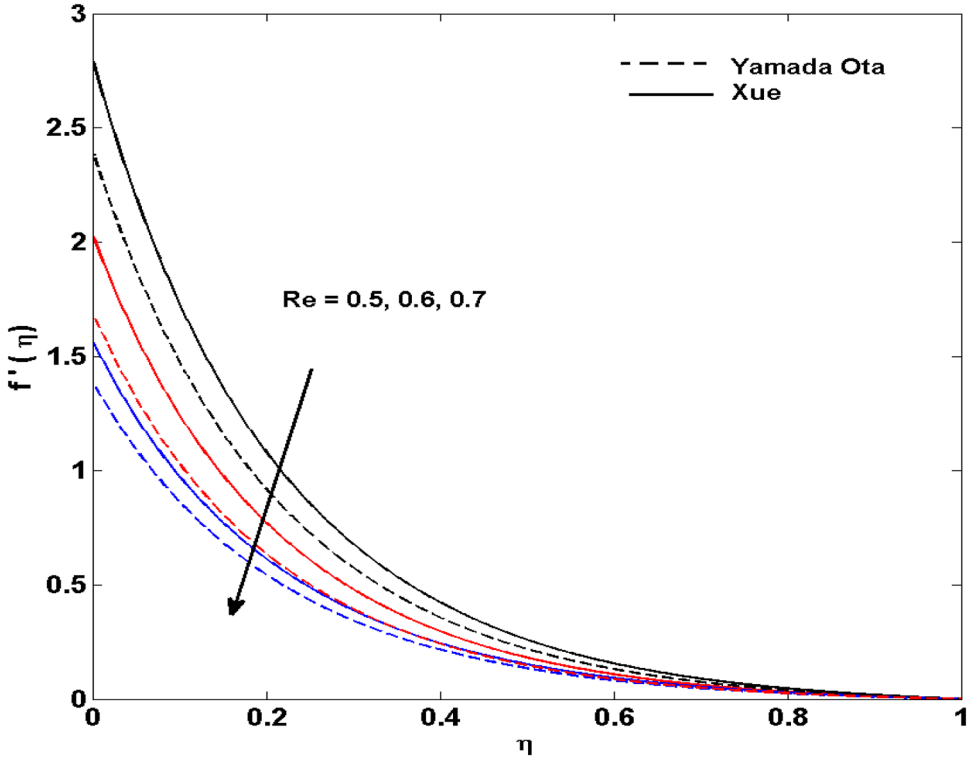

Figure 4. Behaviour of $f'(\eta)$ vs Re. Image generated by using MATLAB 2015a https://www.mathworks.com/help/simulink/release-notes-R2015a.html.

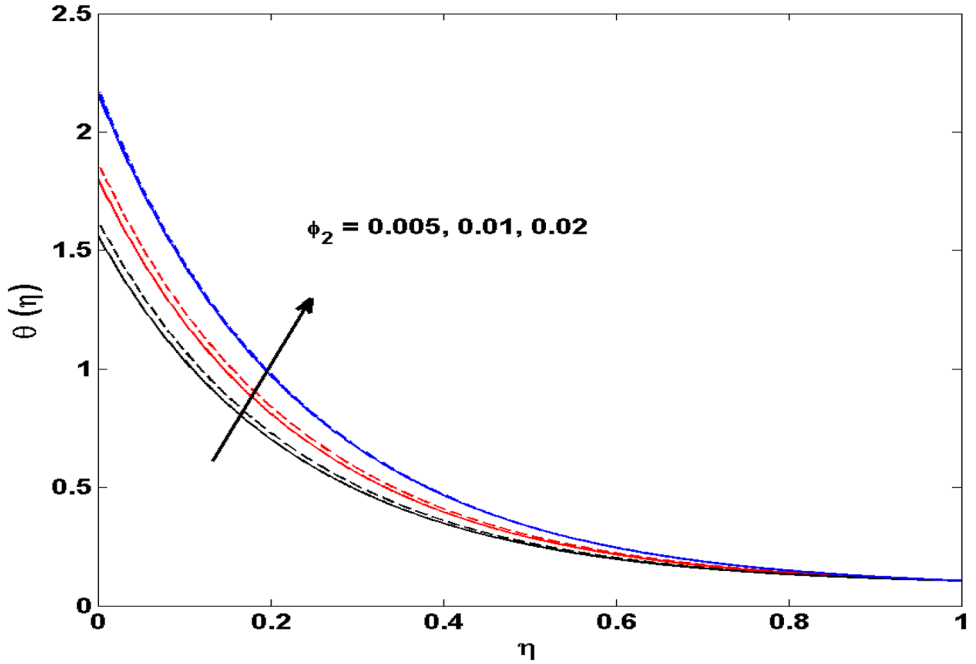

Figure 5. Behaviour of $\theta(\eta)$ vs ϕ_2. Image generated by using MATLAB 2015a https://www.mathworks.com/help/simulink/release-notes-R2015a.html.

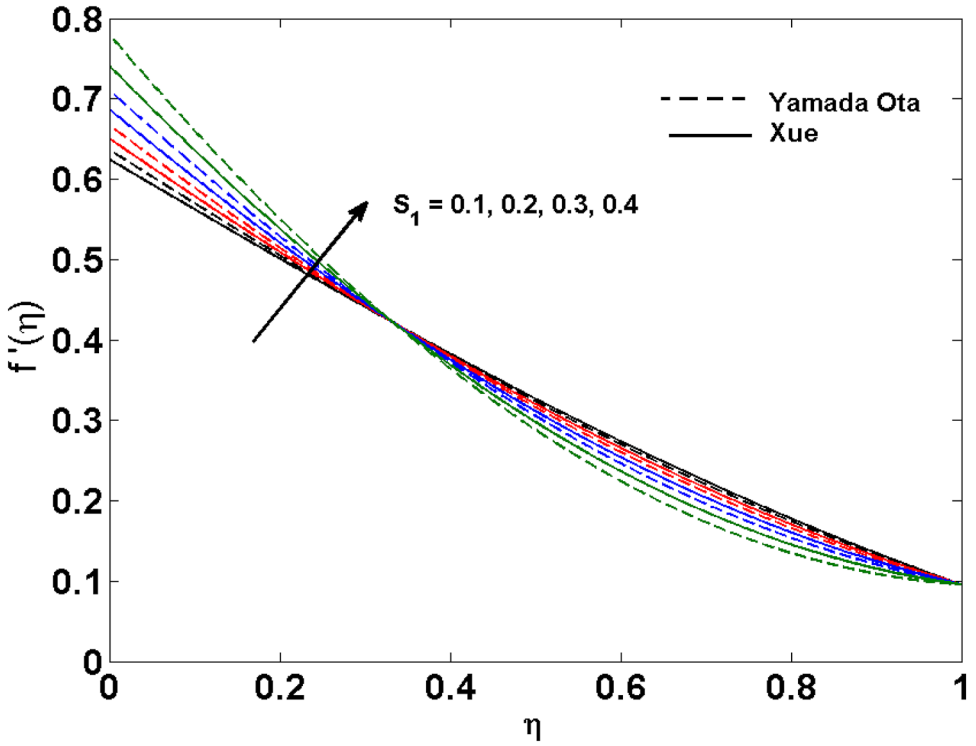

Figure 6. Behaviour of $f'(\eta)$ for S_1. Image generated by using MATLAB 2015a https://www.mathworks.com/help/simulink/release-notes-R2015a.html.

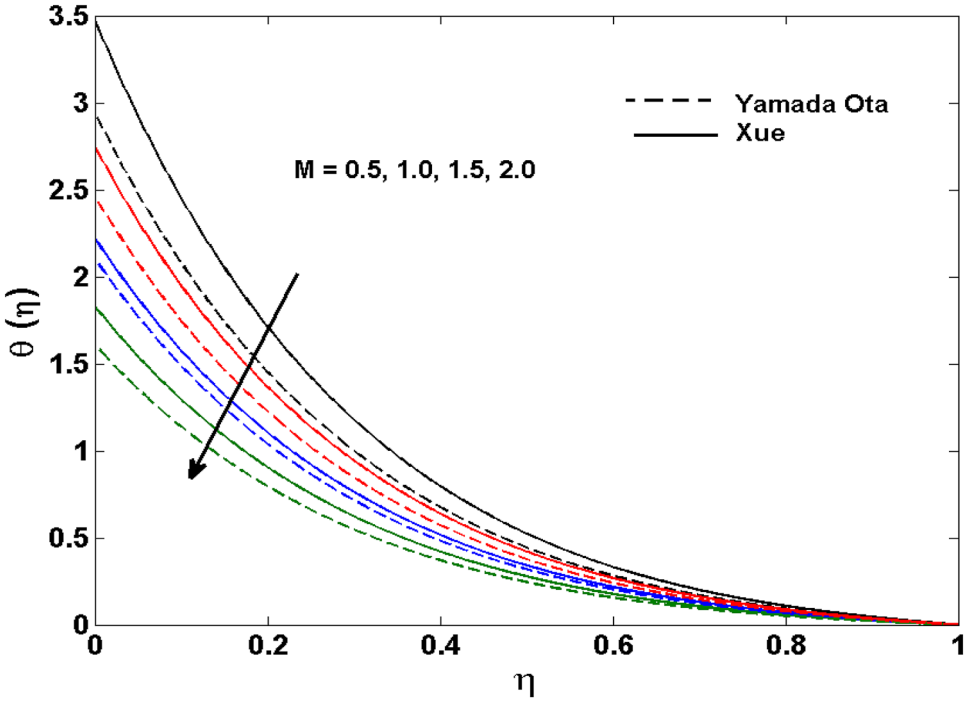

Figure 7. Behaviour of $\theta(\eta)$ vs M. Image generated by using MATLAB 2015a https://www.mathworks.com/help/simulink/release-notes-R2015a.html.

volume fraction (ϕ_2) of multi-walled CNTs. It is understood that thermal profile upsurges when estimations of ϕ_2 are improved. This is because of the fact that by growing the ϕ_2, thermal conductivity upsurges and the thermal boundary layer rises. The influence of the velocity slip parameter (S_1) on the velocity field is given in Fig. 6. It is comprehended that the velocity is at its highest near the surface and it gradually diminishes as it moves away from the surface. The existence of velocity slip within the boundary layer affects the liquid velocity along the sheet to drop, as seen in this diagram. The influences of the thermal slip parameter on the thermal profile of are illustrated in Fig. 7. For higher thermal slip parameter (M) values, the temperature profile decays. Owing to the thermal slip increase in fluid friction with the surface is witnessed which eventually surges the fluid temperature. Furthermore, the dominance of the Yamada-Ota hybrid nanofluid model over the Xue model is obvious here. Figure 8 is shown to witness the relationship between the thermal relaxation parameter (γ) and the thermal profile. It is noticed that the thermal profile reduces for γ. In fact, the material particles take excessive time to shift the heat to the adjacent particles for large γ. Actuality, the material possesses a non-conducting trait for large γ, thus lowering the fluid temperature. Figure 9 is sketched to see the impact of increasing Prandtl number (Pr) versus thermal profile. It is envisioned that as Pr increases, thermal profile reduces. Because the thermal boundary layer thickness reduces for higher Pr. Figure 10 is sketched to see the impact of increasing thermal conductivity parameter (ε_1) versus thermal profile. It is visualized that as ε_1 increases, temperature profile enhances. Physically more amount of heat is being transferred from the surface to the fluid. Consequently, the escalating trend is seen. As we move far away from the surface the thermal conductivity reduces to constant thermal conductivity and hence stops the more increase in the temperature profile. Figure 11 is sketched to address the influence of the heterogeneous parameter (K_s) on the concentration field. It is perceived that the concentration field increases with large estimates of K_s. This impression happens only in the neighborhood of the wall. Figure 12 illustrated the impact of various estimations of the surface-catalyzed parameter (K_{vs}) on the concentration profile. Outcomes specify that an augmentation in the K_{vs} declines the concentration. The boundary layer of concentration becomes denser due to the escalation in K_{vs}. Actually, the rate of surface-catalyzed reaction speeds up with the increase of interface reaction on permeable media, and the rate of mass of species A slowly reaches the lowest at a similar position with constant η. Compared with the porous media (non-catalytic) ($\lambda* = 1,\ K_{vs} = 0$), the concentration of A decreases on the permeable media. This demonstrates the permeable media composed of the same catalyst as the sheet enormously reduces the reaction time. It is observed that when $\lambda* = 0$, physically show that permeable media is absent there, and at this stage, the concentration of species A is higher. It is pertinent to mention here that the influence of the Yamada-Ota hybrid nanofluid model is more dominating than the Xue model. Figure 13 is sketched to address the influence of the heat generation absorption coefficient (Q) on the concentration field. It is perceived that the temperature and relevant thickness have been increases with large estimates of Q. It is observed that when more heat is produced due to Q that is why the temperature field is enlarged. Figures 14, 15, 16 and 17 are depicted to observe the impact of evolving parameters on entropy generation Ns and Bejan number (Be) for both Yamada-Ota and Xue hybrid nanofluid models. In general, the rate of entropy generation is greater for Yamada-Ota than the Xue model. Figure 14 shows the effect of Brinkman

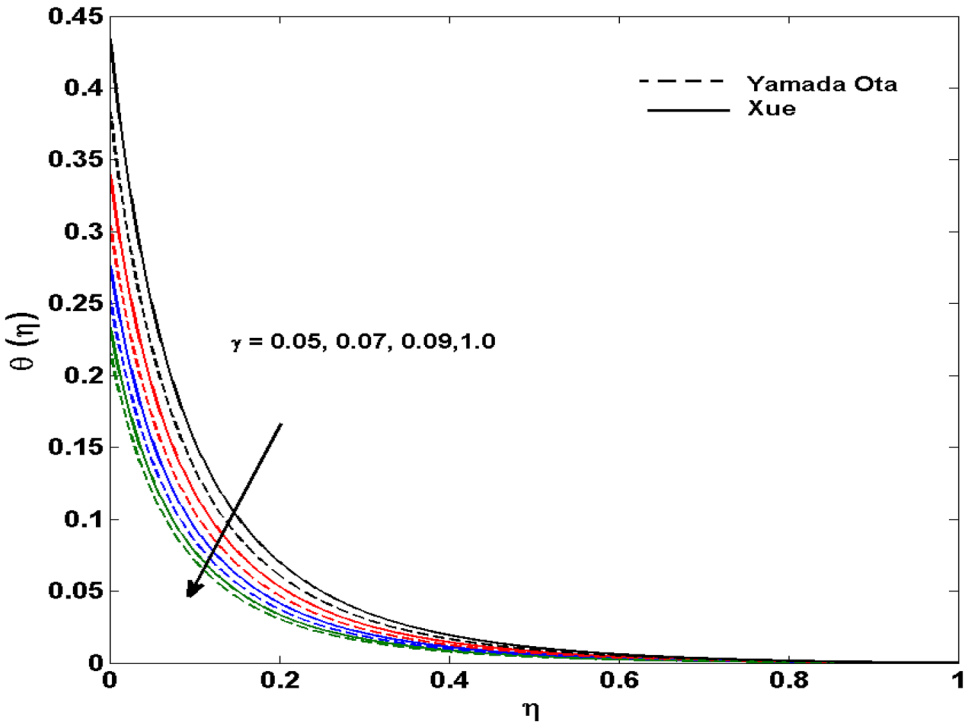

Figure 8. Behaviour of $\theta(\eta)$ vs γ. Image generated by using MATLAB 2015a https://www.mathworks.com/help/simulink/release-notes-R2015a.html.

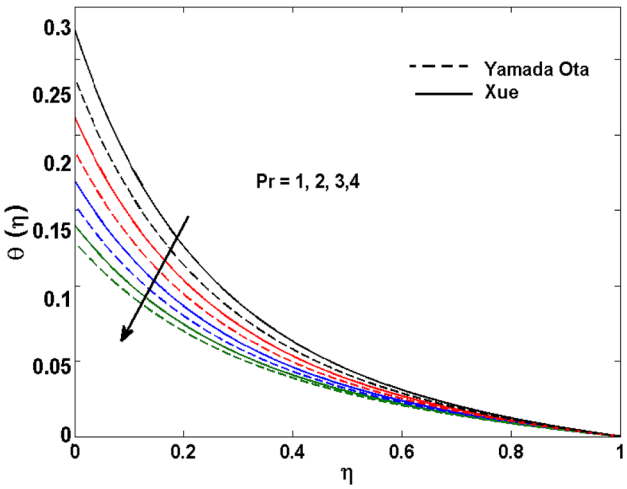

Figure 9. Behaviour of $\theta(\eta)$ vs Pr. Image generated by using MATLAB 2015a https://www.mathworks.com/help/simulink/release-notes-R2015a.html.

number (*Br)* on *Ns*. It is delineated that with an escalation in *Br*, the entropy generation rate increases. Furthermore, an increase in entropy generation rate, caused by friction of fluid and by the mounting values of *Br* Joule dissipation occurs. The effect of Reynolds number (*Re)* on *Be* is expressed in Fig. 15. *Be* increases for high Reynolds number. Due to the increase in *Re* disordered motion occurs and the fluid starts moving more quickly and thus ends up contributing to heightened fluid friction and heat transfer rate affecting the entropy to escalate. Figure 16 shows the effect of *Br* on Be. For greater values of *Br,* the Bejan number reduces. For $Br = 0$, viscous dissipation, irreversibility disappears and only heat transfer irreversibility produce. Higher estimates of porosity parameter ($\lambda*$) cause a decrease in entropy generation rate shown in Fig. 17. Tables 2, 3 and Figs. 18 and 19 display the effects of drag force coefficient for the variation of Re and λ. It is noticed that for higher estimation of Re and λ drag force is rising. It is also noted that the drag force is superior for the Yamada-Ota model than for the Xue model. Here, the Yamada-Ota model attains a faster heat transfer rate than the Xue model. Table 4 and

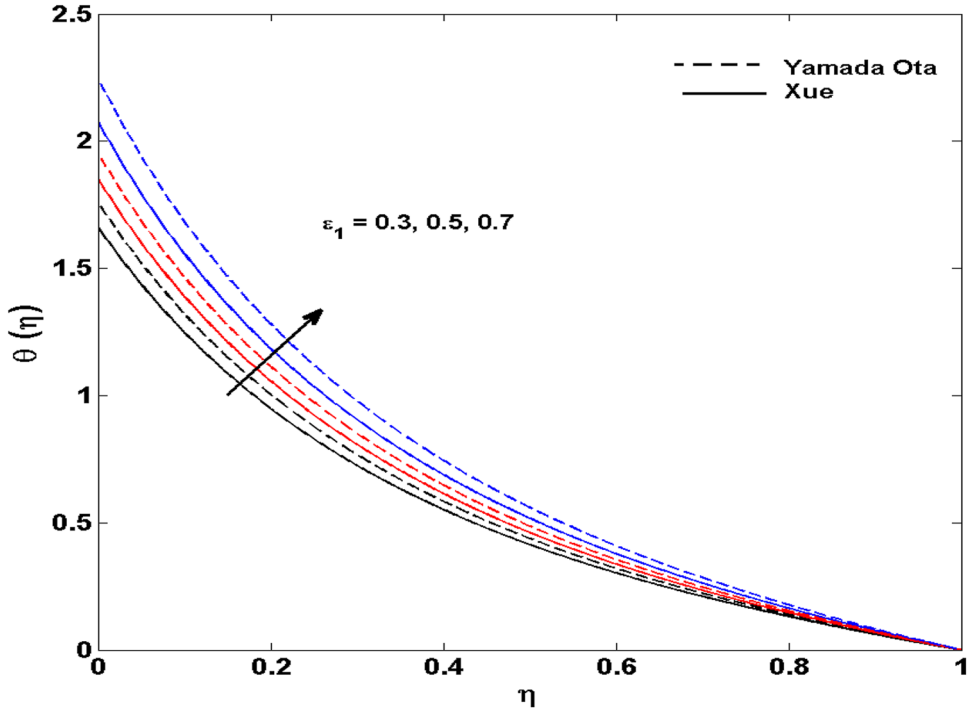

Figure 10. Behaviour of $\theta(\eta)$ vs ε_1. Image generated by using MATLAB 2015a https://www.mathworks.com/help/simulink/release-notes-R2015a.html.

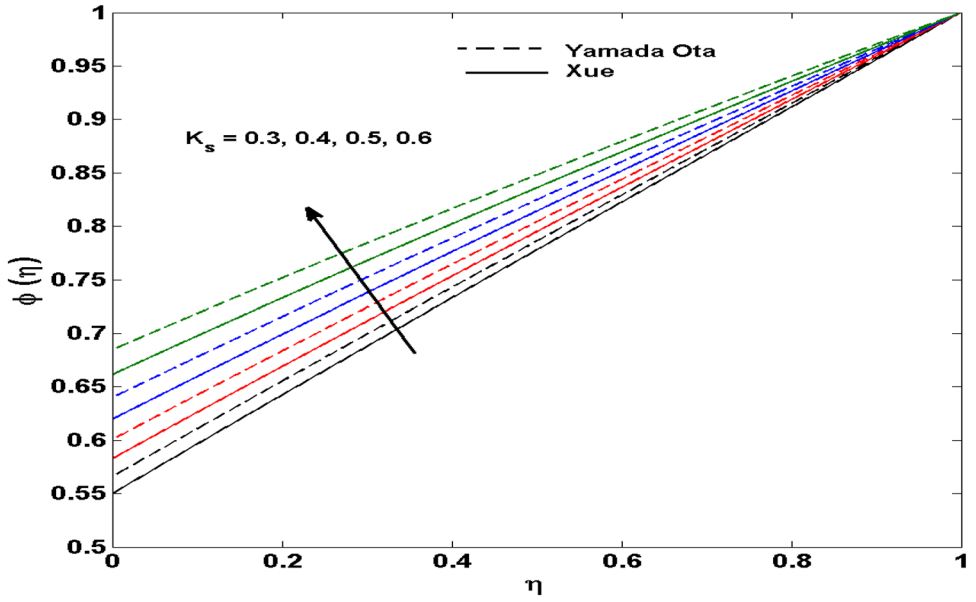

Figure 11. Behaviour of $\phi(\eta)$ vs K_s. Image generated by using MATLAB 2015a https://www.mathworks.com/help/simulink/release-notes-R2015a.html.

Fig. 20 display the effects of heat transfer rate for the variation of Pr. It is observed that for higher estimation of Pr heat transfer rate is increases.

Table 5 and Fig. 21 display the effects of mass transfer rate for the variation of Schmidt number *Sc*. It is noticed that for higher estimation of *Sc* mass transfer rate is reduces.

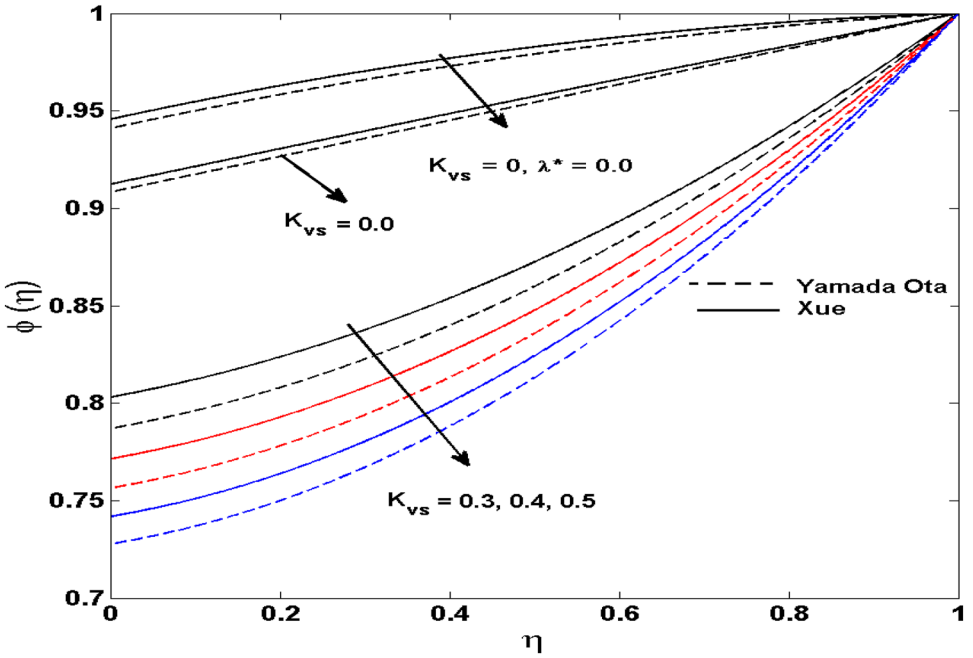

Figure 12. Behaviour of $\phi(\eta)$ vs K_{vs}. Image generated by using MATLAB 2015a https://www.mathworks.com/help/simulink/release-notes-R2015a.html.

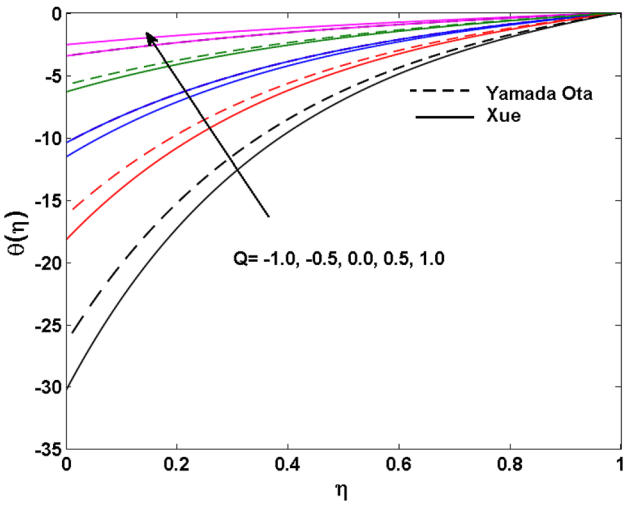

Figure 13. Behaviour of $\theta(\eta)$ vs Q. Image generated by using MATLAB 2015a https://www.mathworks.com/help/simulink/release-notes-R2015a.html.

Final remarks

In this study, we have examined the hybrid nanofluid flow (SWCNTs-MWCNTs/Ethelyn glycol) with Yamada-Ota and Xue model in a rotating channel with C–C heat flux. The heat source/sink, slip effects, with the surface catalyzed reaction amalgamated with HOM-HET chemical reactions are also considered. The entropy generation analysis is also considered for the said hybrid nanofluid flow in the specific geometry. The problem is addressed numerically. The noteworthy observations of the model are appended as given below:

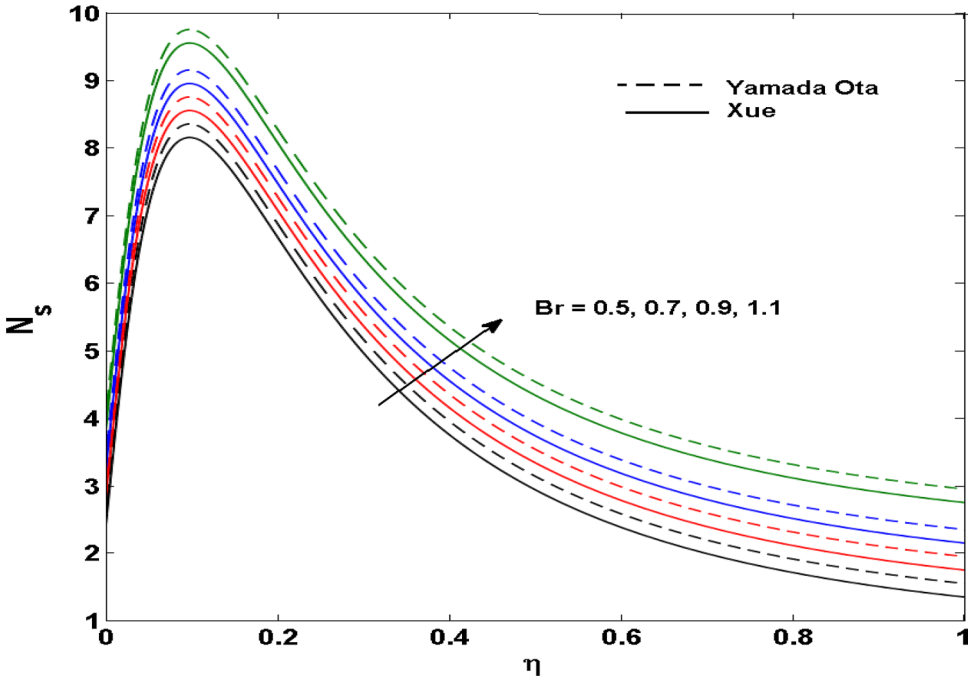

Figure 14. Behaviour of *Ns* vs *Br*. Image generated by using MATLAB 2015a https://www.mathworks.com/help/simulink/release-notes-R2015a.html.

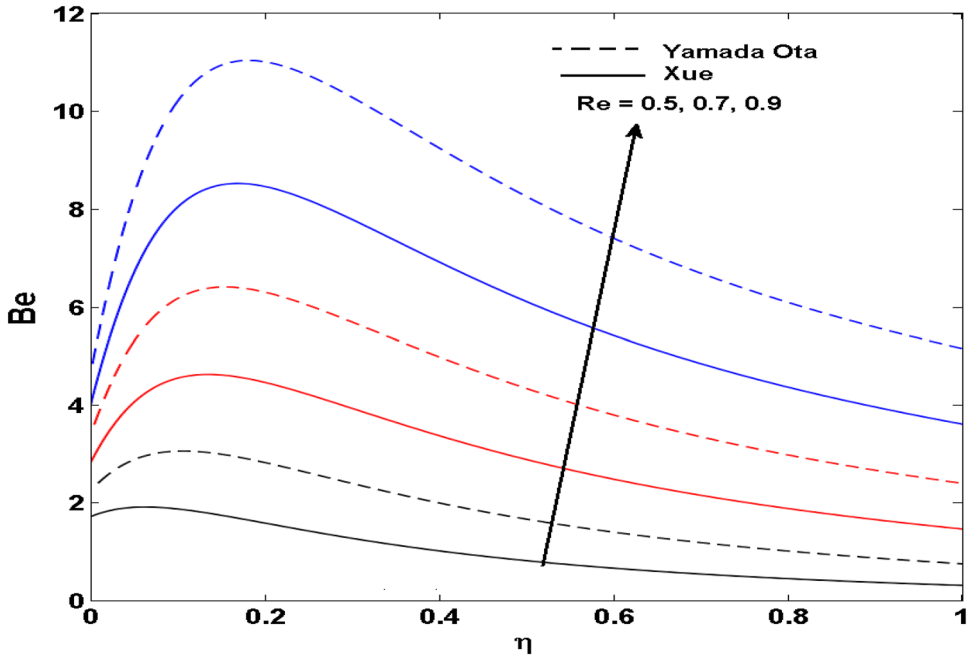

Figure 15. Behaviour of *Be* vs Re. Image generated by using MATLAB 2015a https://www.mathworks.com/help/simulink/release-notes-R2015a.html.

- The fluid velocity is diminished for the higher rotation while an opposing trend is witnessed for the strong slip.
- Higher estimations of the surface-catalyzed parameter cause reduction in the fluid concentration. However, the temperature profile is reduced for the thermal relaxation parameter.
- The dominance of the Yamada-Ota hybrid nanofluid model is obvious in comparison to the Xue model.

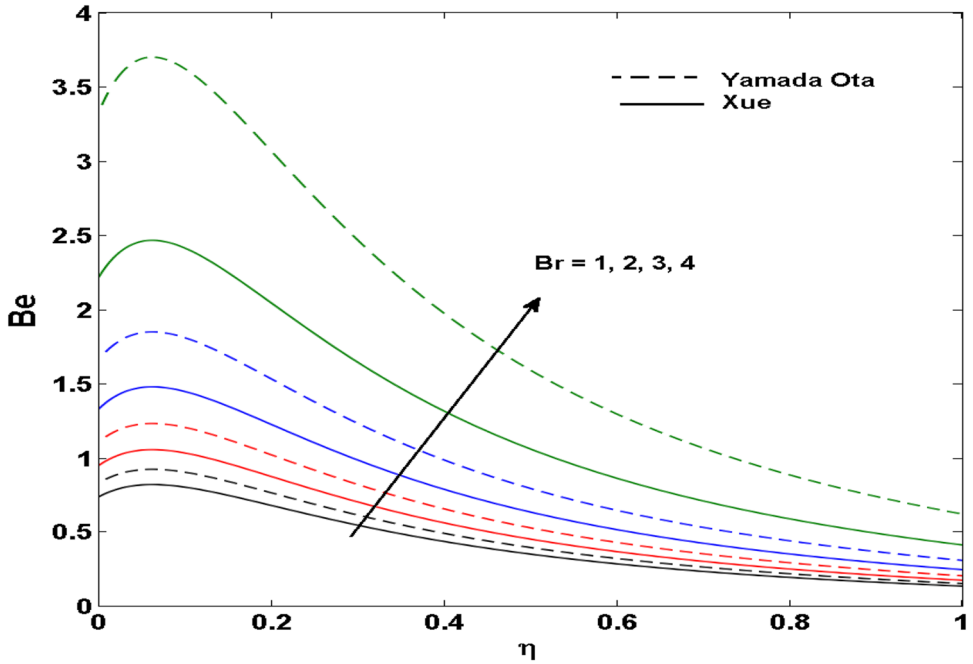

Figure 16. Behaviour of *Be* vs *Br*. Image generated by using MATLAB 2015a https://www.mathworks.com/help/simulink/release-notes-R2015a.html.

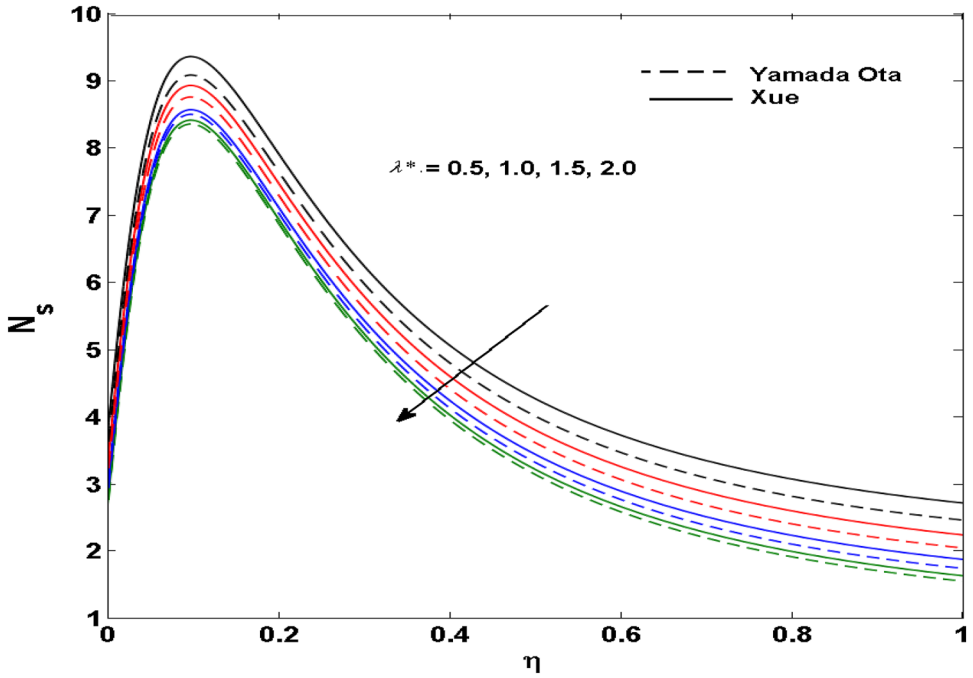

Figure 17. Variation of *Ns* vs $\lambda*$. Image generated by using MATLAB 2015a https://www.mathworks.com/help/simulink/release-notes-R2015a.html.

- Large estimates of the Reynolds number and porosity parameter affect the entropy generation rate.
- The heat and mass transfer rates increase and decrease for large estimates of the Prandtl and Schmidt numbers respectively.

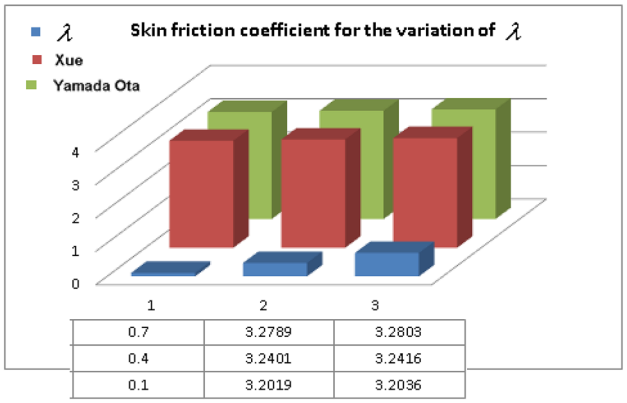

Figure 18. $F''(0)$ for λ. Image generated by using MATLAB 2015a https://www.mathworks.com/help/simulink/release-notes-R2015a.html.

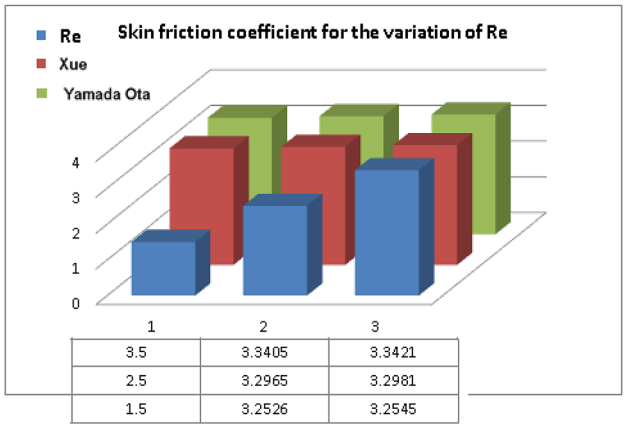

Figure 19. $F''(0)$ for Re. Image generated by using MATLAB 2015a https://www.mathworks.com/help/simulink/release-notes-R2015a.html.

Pr	$Nu_x\sqrt{\mathrm{Re}_x}$	
	Xue model	Yamada-Ota model
2	4691.3	5071.3
3	4908.4	5316.5
4	5255.9	5743.3
5	5858.8	6006.1

Table 4. Numerical result of $Nu_x\sqrt{\mathrm{Re}_x}$ for Pr.

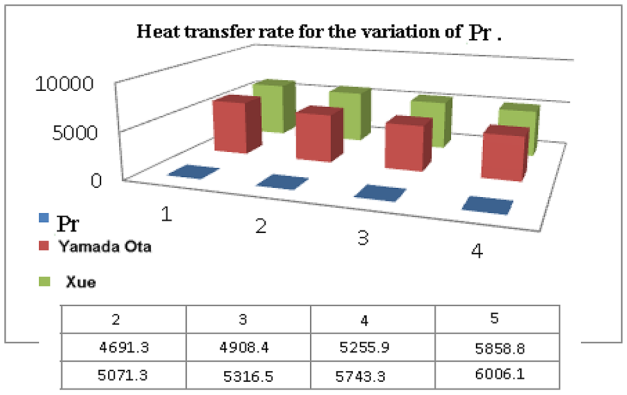

Figure 20. Heat transfer rate for the variation of Pr.

Sc	$Sh_x\sqrt{\mathrm{Re}_x}$	
	Xue model	Yamada-Ota model
0.4	0.11134	0.23546
0.5	0.10447	0.21632
0.6	0.09303	0.19857
0.7	0.08183	0.16398

Table 5. Numerical estimation of $Sh_x\sqrt{\mathrm{Re}_x}$ for *Sc*.

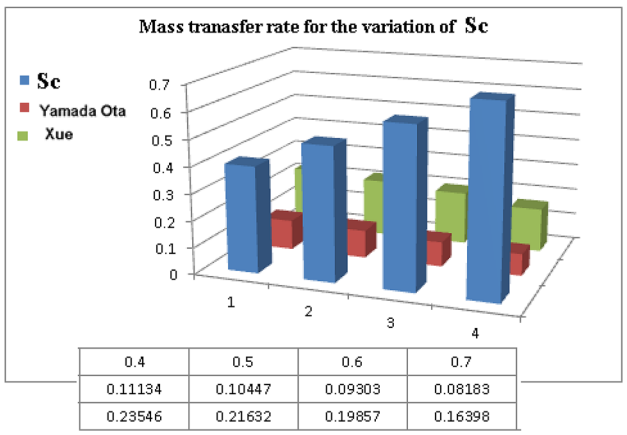

Figure 21. Mass transfer rate for the variation of *Sc*.

Received: 20 June 2021; Accepted: 30 August 2021
Published online: 01 October 2021

References

1. Acharya, N., Das, K. & Kundu, P. K. Rotating flow of carbon nanotube over a stretching surface in the presence of magnetic field: a comparative study. *Appl. Nanosci.* **8**(3), 369–378 (2018).
2. Dawar, A., Shah, Z., Khan, W., Idrees, M. & Islam, S. Unsteady squeezing flow of magnetohydrodynamic carbon nanotube nanofluid in rotating channels with entropy generation and viscous dissipation. *Adv. Mech. Eng.* **11**(1), 1687814018823100 (2019).
3. Kumar, A., Tripathi, R., Singh, R. & Seth, G. S. Three-dimensional magnetohydrodynamic flow of micropolar CNT-based nanofluid through a horizontal rotating channel: OHAM analysis. *Indian J. Phys.* **94**(3), 319–332 (2020).
4. Pandit, S., & Sharma, S. Wavelet strategy for flow and heat transfer in CNT-water based fluid with asymmetric variable rectangular porous channel. *Eng. Comput.* 1–11 (2020).
5. Khan, U., Ahmed, N. & Mohyud-Din, S. T. Numerical investigation for three dimensional squeezing flow of nanofluid in a rotating channel with lower stretching wall suspended by carbon nanotubes. *Appl. Therm. Eng.* **113**, 1107–1117 (2017).
6. Bilal, M., Arshad, H., Ramzan, M., Shah, Z. & Kumam, P. Unsteady hybrid-nanofluid flow comprising ferrousoxide and CNTs through porous horizontal channel with dilating/squeezing walls. *Sci. Rep.* **11**(1), 1–16 (2021).
7. Ramzan, M., Chung, J. D., Kadry, S., Chu, Y. M. & Akhtar, M. Nanofluid flow containing carbon nanotubes with quartic autocatalytic chemical reaction and Thompson and Troian slip at the boundary. *Sci. Rep.* **10**(1), 1–13 (2020).
8. Khan, U. *et al.* Numerical simulation of Darcy–Forchheimer 3D unsteady nanofluid flow comprising carbon nanotubes with Cattaneo-Christov heat flux and velocity and thermal slip conditions. *Processes* **7**(10), 687 (2019).
9. Bilal, M. & Ramzan, M. Hall current effect on unsteady rotational flow of carbon nanotubes with dust particles and nonlinear thermal radiation in Darcy-Forchheimer porous media. *J. Therm. Anal. Calorim.* **138**(5), 3127–3137 (2019).
10. Ramzan, M., Abid, N., Lu, D. & Tlili, I. Impact of melting heat transfer in the time-dependent squeezing nanofluid flow containing carbon nanotubes in a Darcy–Forchheimer porous media with Cattaneo-Christov heat flux. *Commun. Theor. Phys.* **72**(8), 085801 (2020).
11. Baron de Fourier, J. B. J. Théorie analytique de la chaleur. Firmin Didot (1822).
12. Cattaneo, C. Sulla conduzione del calore. *Atti Sem. Mat. Fis. Univ. Modena* **3**, 83–101 (1948).
13. Christov, C. I. On frame indifferent formulation of the Maxwell–Cattaneo model of finite-speed heat conduction. *Mech. Res. Commun.* **36**(4), 481–486 (2009).
14. Ramzan, M., Gul, H. & Kadry, S. Onset of Cattaneo–Christov heat flux and thermal stratification in ethylene-glycol-based nanofluid flow containing carbon nanotubes in a rotating frame. *IEEE Access* **7**, 146190–146197 (2019).
15. Hayat, T., Muhammad, K., Farooq, M. & Alsaedi, A. Squeezed flow subject to Cattaneo–Christov heat flux and rotating frame. *J. Mol. Liq.* **220**, 216–222 (2016).
16. Karim, M. E. & Samad, M. A. Effect of Brownian diffusion on squeezing elastico-viscous nanofluid flow with Cattaneo–Christov heat flux model in a channel with double slip effect. *Appl. Math.* **11**(4), 277–291 (2020).
17. Ramzan, M., Gul, H., Kadry, S. & Chu, Y. M. Role of bioconvection in a three dimensional tangent hyperbolic partially ionized magnetized nanofluid flow with Cattaneo-Christov heat flux and activation energy. *Int. Commun. Heat Mass Transf.* 104994 (2020).
18. Ramzan, M., Riasat, S., Shah, Z., Kumam, P. & Thounthong, P. Unsteady MHD carbon nanotubes suspended nanofluid flow with thermal stratification and nonlinear thermal radiation. *Alex. Eng. J.* **59**(3), 1557–1566 (2020).
19. Shaheen, N., Ramzan, M., Alshehri, A., Shah, Z. & Kumam, P. Soret-Dufour impact on a three-dimensional Casson nanofluid flow with dust particles and variable characteristics in a permeable media. *Sci. Rep.* **11**(1), 1–21 (2021).
20. Ahmad, S., Nadeem, S., Muhammad, N. & Khan, M. N. Cattaneo–Christov heat flux model for stagnation point flow of micropolar nanofluid toward a nonlinear stretching surface with slip effects. *J. Thermal Anal. Calorim.* **143**, 1–1 (2020).
21. Zhang, Y., Shahmir, N., Ramzan, M., Alotaibi, H. & Aljohani, H. M. Upshot of melting heat transfer in a Von Karman rotating flow of gold-silver/engine oil hybrid nanofluid with cattaneo-christov heat flux. *Case Stud. Therm. Eng.* 101149 (2021).
22. Gul, H., Ramzan, M., Chung, J. D., Chu, Y. M. & Kadry, S. Multiple slips impact in the MHD hybrid nanofluid flow with Cattaneo–Christov heat flux and autocatalytic chemical reaction. *Sci. Rep.* **11**(1), 1–14 (2021).
23. Ramzan, M. & Shaheen, N. Thermally stratified Darcy–Forchheimer nanofluid flow comprising carbon nanotubes with effects of Cattaneo–Christov heat flux and homogeneous–heterogeneous reactions. *Phys. Scr.* **95**(1), 015701 (2019).
24. Hayat, T., Muhammad, K., Alsaedi, A. & Farooq, M. Features of Darcy–Forchheimer flow of carbon nanofluid in frame of chemical species with numerical significance. *J. Cent. South Univ.* **26**(5), 1260–1270 (2019).
25. Ramzan, M., Gul, H. & Sheikholeslami, M. Effect of second order slip condition on the flow of tangent hyperbolic fluid—a novel perception of Cattaneo–Christov heat flux. *Phys. Scr.* **94**(11), 115 (2019).
26. Ramzan, M., Sheikholeslami, M., Saeed, M. & Chung, J. D. On the convective heat and zero nanoparticle mass flux conditions in the flow of 3D MHD couple Stress nanofluid over an exponentially stretched surface. *Sci. Rep.* **9**(1), 562 (2019).
27. Ramzan, M., Bilal, M., Chung, J. D. & Mann, A. B. On MHD radiative Jeffery nanofluid flow with convective heat and mass boundary conditions. *Neural Comput. Appl.* **30**(9), 2739–2748 (2018).
28. Imtiaz, M., Hayat, T., Alsaedi, A. & Ahmad, B. Convective flow of carbon nanotubes between rotating stretchable disks with thermal radiation effects. *Int. J. Heat Mass Transf.* **101**, 948–957 (2016).
29. Jain, S. & Gupta, P. Flow and heat transfer of carbon nanotubes nanofluid flow over a 3-d inclined nonlinear stretching sheet with porous media. In *Numerical Heat Transfer and Fluid Flow* (pp. 321–329). (Springer, 2019).
30. Jain, S. & Gupta, P. Flow and heat transfer of carbon nanotubes nanofluid flow over a 3-D inclined nonlinear stretching sheet. *Numer. Heat Transf. Fluid Flow: Select Proc. NHTFF* **2018**, 321 (2019).
31. Jain, S. & Gupta, P.. Numerical study of water-based carbon nanotubes' nanofluid flow over a nonlinear inclined 3-D stretching sheet for homogeneous–heterogeneous reactions with porous media. In *Engineering Vibration, Communication and Information Processing* (pp. 633–649). (Springer, 2019).
32. Basha, H. T., Animasaun, I. L., Makinde, O. D. & Sivaraj, R. Effect of electromagnetohydrodynamic on chemically reacting nanofluid flow over a cone and plate. In *Applied Mathematics and Scientific Computing* (pp. 99–107) (2019).
33. Kumam, P., Shah, Z., Dawar, A., Rasheed, H. U. & Islam, S. (2019). Entropy generation in MHD radiative flow of CNTs Casson nanofluid in rotating channels with heat source/sink. *Mathematical Problems in Engineering* (2019).
34. Abbas, N., Malik, M. Y., Nadeem, S. & Alarifi, I. M. On extended version of Yamada-Ota and Xue models of hybrid nanofluid on moving needle. *The Eur. Phys. J. Plus* **135**(2), 1–16 (2020).
35. Riasat, S., Ramzan, M., Sun, Y. L., Malik, M. Y. & Chinram, R. Comparative analysis of Yamada-Ota and Xue models for hybrid nanofluid flow amid two concentric spinning disks with variable thermophysical characteristics. *Case Stud. Therm. Eng.* **26**, 101039 (2021).
36. Khan, M., Ijaz, T., Hayat, A., Alsaedi, S. Q. & Tamoor, M. Entropy optimization and quartic autocatalysis in MHD chemically reactive stagnation point flow of Sisko nanomaterial. *Int. J. Heat Mass Transf.* **129**, 1329–1329 (2019).

Acknowledgements
The authors extend their appreciation to the Deanship of Scientific Research at King Khalid University, Abha 61413, Saudi Arabia for funding this work through research groups program under grant number RGP-2/13/42.

Author contributions
M.R. did conceptualization, H. G. worked on methodology and wrote the original draft, M.Y.M. did validation of the draft. D.B. and K.S.N. helped in revising the manuscript and arrangement of funds.

Competing interests
The authors declare no competing interests.

Additional information
Correspondence and requests for materials should be addressed to M.R.

Reprints and permissions information is available at www.nature.com/reprints.

Publisher's note Springer Nature remains neutral with regard to jurisdictional claims in published maps and institutional affiliations.